ACSNANO

www.acsnano.org

ARTICLE

Toward Engineering Intrinsic Line Widths and Line Broadening in Perovskite Nanoplatelets

Albert Liu, Gabriel Nagamine, Luiz G. Bonato, Diogo B. Almeida, Luiz F. Zagonel, Ana F. Nogueira, Lazaro A. Padilha,* and Steven T. Cundiff*

Cite This: *ACS Nano* 2021, 15, 6499–6506

Read Online

ACCESS | Metrics & More | Article Recommendations | Supporting Information

ABSTRACT: **Perovskite nanoplatelets possess extremely narrow absorption and emission line widths, which are crucial characteristics for many optical applications. However, their underlying intrinsic and extrinsic line-broadening mechanisms are poorly understood. Here, we apply multidimensional coherent spectroscopy to determine the homogeneous line broadening of colloidal perovskite nanoplatelet ensembles. We demonstrate a dependence of not only their intrinsic line widths but also of various broadening mechanisms on platelet geometry. We find that decreasing nanoplatelet thickness by a single monolayer results in a 2-fold reduction of the inhomogeneous line width and a 3-fold reduction of the intrinsic homogeneous line width to the sub-millielectronvolts regime. In addition, our measurements suggest homogeneously broadened exciton resonances in two-layer (but not necessarily three-layer) nanoplatelets at room-temperature.**

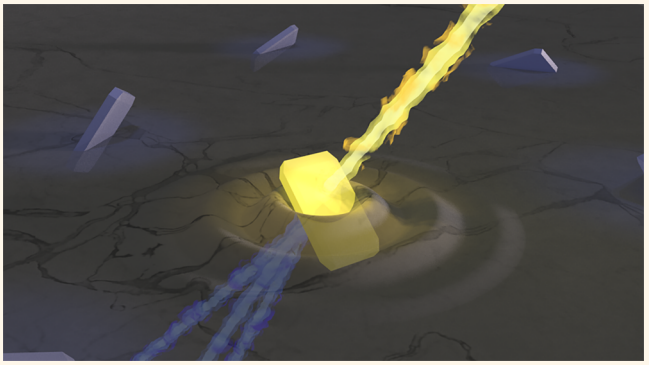

KEYWORDS: *semiconductor nanocrystals, lead-halide perovskites, homogeneous line broadening, multidimensional coherent spectroscopy, electron−phonon coupling, excitation-induced dephasing*

Metal halide perovskites are a class of materials that have attracted tremendous interest in recent years due to their superior performance in electronic transport and optical interactions.[1−4] In particular, lead halide perovskite nanocrystals have generated much excitement due to their light absorption and emission properties.[5,6]

Although perovskite nanocrystals were initially limited to nanocube geometries, synthesis of perovskite nanoplatelets was achieved shortly thereafter.[7,8] Perovskite nanoplatelets share the efficient and tunable photophysics of their nanocube counterparts while possessing useful characteristics of their own. Their planar geometry allows for directional light absorption/emission[9] and efficient energy transfer in stacked superlattices,[10] while precise control of the monolayer thickness (more precisely each layer formed by Pb-halide tetrahedra) results in homogeneity in the dominant out-of-plane quantum confinement.[11] Because the absorption and emission energy of nanoplatelets are predominantly determined by the nanoplatelet thickness, variation in lateral confinement of electronic excitations is commonly believed to be negligible.

However, many practical applications of colloidal nanoplatelets are still hampered by spectral broadening due to size and shape dispersion, known as inhomogeneous broadening. For example, overlap of absorption and emission bands of nanoplatelet ensembles degrades their efficiency as lasing media.[12] Inhomogeneous broadening also obscures the intrinsic homogeneous line width in absorption and luminescence measurements, a fundamental metric for many optoelectronic applications. In particular, elucidating the dominant homogeneous broadening mechanisms is crucial for optimizing energy transfer efficiencies of nanoplatelet superlattices.[10,11] To properly determine the homogeneous and inhomogeneous line widths and determine their underlying broadening mechanisms, a more advanced nonlinear spectroscopic technique is required to separate and characterize the two contributions to line width broadening.

By correlating absorption and emission spectra, multidimensional coherent spectroscopy (MDCS)[13] is able to separate homogeneous and inhomogeneous broadening mechanisms

Received: November 4, 2020
Accepted: March 19, 2021
Published: March 26, 2021

Downloaded via BROOKHAVEN NATL LABORATORY on February 10, 2025 at 19:53:36 (UTC).
See https://pubs.acs.org/sharingguidelines for options on how to legitimately share published articles.

ACS Publications

© 2021 American Chemical Society

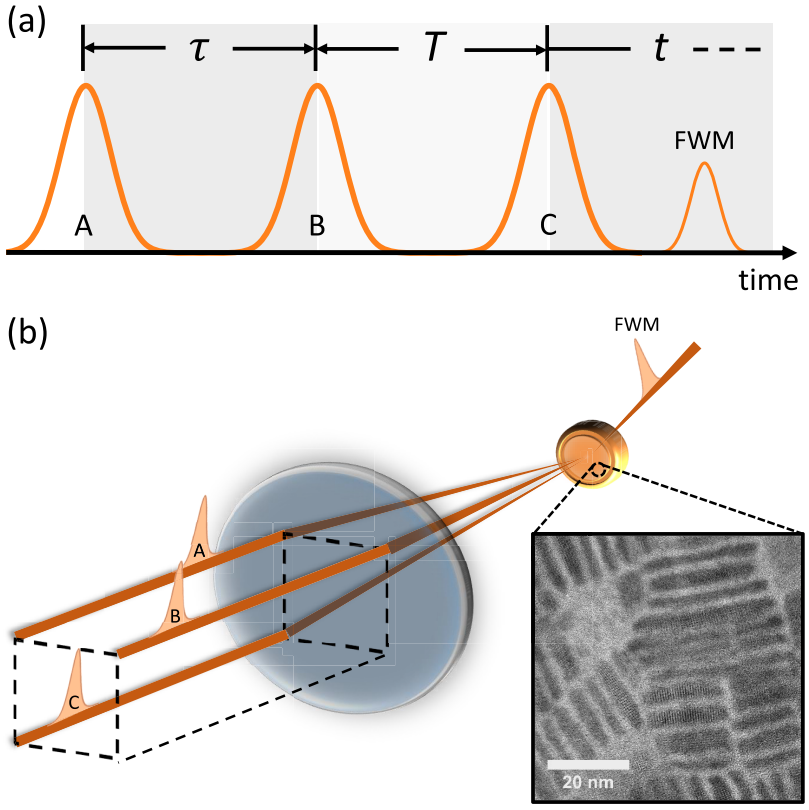

Figure 1. (a) Diagram defining the time-delays τ, T, and t that we Fourier transform along to generate an MDCS spectrum. (b) Experimental schematic, consisting of three phase-stable laser pulses arranged in the box geometry that generate a photon echo. Inset shows transmission electron microscopy image of studied 170 °C nanoplatelets (MDCS measurements are performed on a colloidal suspension).

into orthogonal directions in a multidimensional spectrum. In particular, the ability of MDCS to circumvent inhomogeneous broadening has already proven invaluable in studying the homogeneous properties of colloidal nanoparticles.[14−19] In this work, we apply MDCS at cryogenic temperatures to simultaneously determine the homogeneous and inhomogeneous line widths of two-layer and three-layer $CsPbI_3$ perovskite nanoplatelet ensembles. We find that a change in thickness by a single layer drastically changes the degrees of both homogeneous and inhomogeneous broadening. Temperature- and excitation power-dependent measurements reveal the dominant line width broadening mechanisms to be acoustic phonon coupling and excitation induced dephasing (EID). By extrapolating their linear line width temperature dependences, we expect homogeneously broadened exciton resonances in two-layer nanoplatelets at room temperature but not necessarily for thicker nanoplatelets.

RESULTS AND DISCUSSION

To perform MDCS we use a multi-dimensional optical nonlinear spectrometer[20] in which three phase-stabilized laser pulses generate a nonlinear four-wave-mixing (FWM) signal as a function of three time delays τ, T, and t (shown in Figure 1a). Fourier transforming the FWM signal as a function of delays τ and t then generates a two-dimensional (2D) spectra (with conjugate axes $\hbar\omega_\tau$ and $\hbar\omega_t$) which correlates absorption and emission dynamics.[16,17]

In 2D spectra, inhomogeneous and homogeneous broadening manifest as broadening in the diagonal ($|\hbar\omega_\tau| = |\hbar\omega_t|$) and orthogonal cross-diagonal directions, respectively.[21] We note that a time-integrated FWM study has been performed on $MAPbI_3$ nanoplatelets to extract the homogeneous line width at a single temperature and excitation density,[22] but such measurements return a single ensemble-averaged value for the homogeneous line width and provide no information about its variation across the inhomogeneous distribution. In contrast, the cross-diagonal line shape of a 2D spectrum at a given position along the diagonal $\hbar\omega_{CD} = |\hbar\omega_\tau| = |\hbar\omega_t|$ reflects the ensemble-averaged homogeneous response of nanoplatelets with a resonance energy $\hbar\omega_{CD}$. Fitting the diagonal and cross-diagonal lineshapes simultaneously[21] then provides the homogeneous and inhomogeneous line widths ($\gamma = \frac{\hbar}{T_2}$ and σ, respectively). Here, our 2D spectra are acquired at $T = 1$ ps, to preclude effects of subpicosecond population relaxation and pulse-overlap effects. However, because the nanoplatelet absorption line widths exceed the widths of our excitation spectra, the diagonal line widths in our 2D spectra do not represent the total inhomogeneous distribution of nanoplatelet resonance energies. To prevent distortion of fitted homogeneous line widths by such finite pulse bandwidth effects, we further divide out the experimental excitation spectrum for each 2D spectrum.[23,24]

The exciton Bohr diameter in bulk $CsPbI_3$ is 12 nm[25] and thus for nanoplatelets comprised of few monolayers the absorption and photoluminescence peaks are predominantly determined by the nanoplatelet thickness (only weakly dependent on the lateral size). This results in spectrally well-separated peaks as previously demonstrated by us and others.[8,26,27] Both two-layer and three-layer thick nanoplatelets were synthesized at a reaction temperature of 170 °C, as evident from the appearance of two distinct peaks in low-

https://doi.org/10.1021/acsnano.0c09244
ACS Nano 2021, 15, 6499−6506

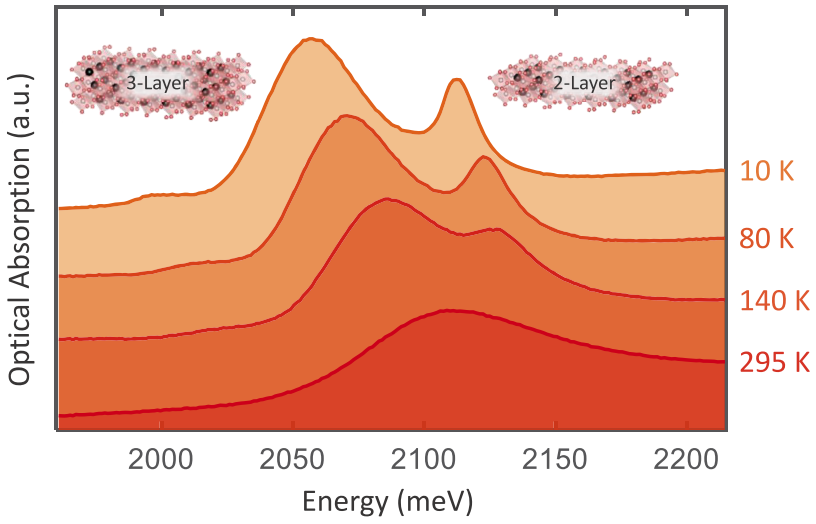

Figure 2. Temperature-dependent absorption spectra of nanoplatelets synthesized at 170 °C. A single broad absorption peak is visible at room temperature, which splits into two distinct peaks attributed to different layer thicknesses at cryogenic temperatures.

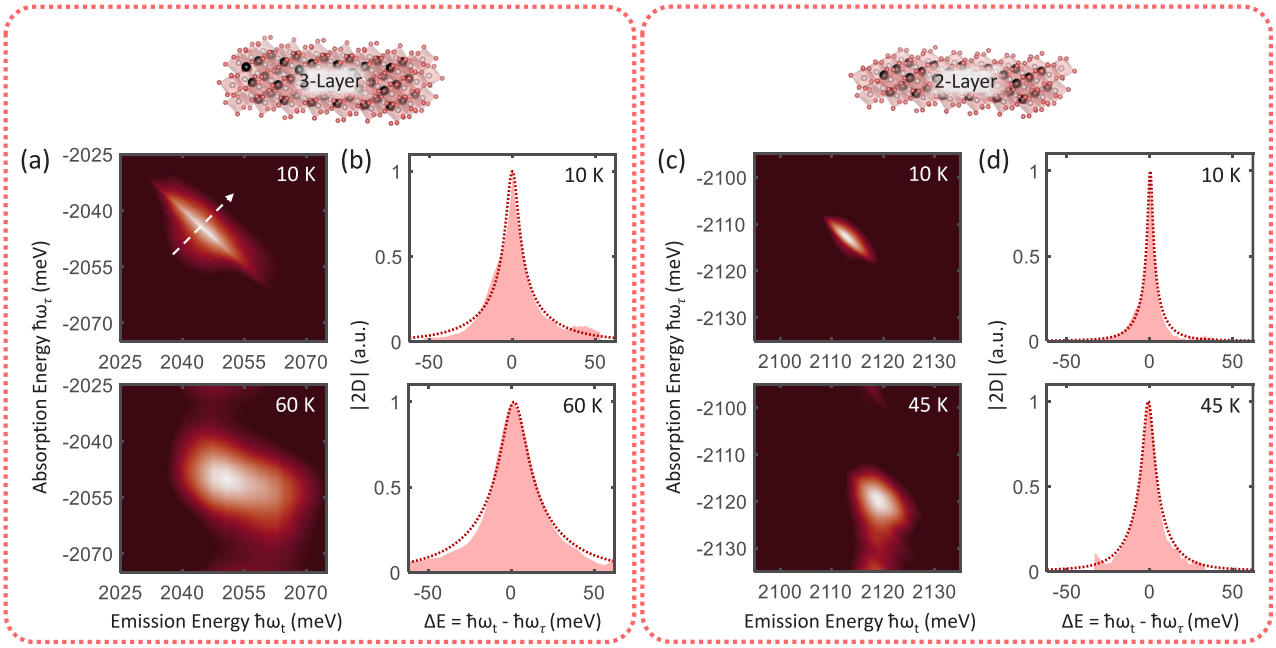

Figure 3. (a,c) Magnitude 2D spectra of (a) three-layer and (c) two-layer nanoplatelets synthesized at a reaction temperature of 170 °C and acquired with excitation densities N_X = 1.753 × 10^{13} and 1.875 × 10^{13} cm^{-2}, respectively, at the indicated temperatures. The waiting time was set to T = 1 ps to avoid coherent signals during pulse overlap. (b,d) Cross-diagonal slices of the (b) three-layer and (d) two-layer 2D spectra centered at 2045 and 2113 meV, respectively. The cross-diagonal slice location for the 10 K slice in (b) is indicated by the white dashed arrow in (a). Experimental data and line shape fits are plotted as the shaded area plots and dotted lines, respectively.

temperature absorption spectra shown in Figure 2 (see Supporting Information). The additional peak should be distinguished from those of other origins such as light-hole/heavy-hole splitting in CdSe nanoplatelets[28] (which is not relevant in the single-valence band structure in $CsPbI_3$[29]) or internanocrystal coupling (which should be negligible in the dilute colloidal suspensions studied here). Measurements were also performed on three-layer nanoplatelets synthesized at a reaction temperature of 110 °C, from which no spectral contribution from two-layer nanoplatelets was observed (see Supporting Information for low-temperature absorption spectra). Although photoluminescence spectra of these samples indicate the presence of even thicker nanoplatelets, their resonance energies lie outside of the tuning range of our laser source and are not accessible in our current experimental setup.

Transmission electron microscopy (TEM) measurements performed on each sample inform average lateral edge lengths of 10.7 ± 2.3 and 12.4 ± 2.0 nm for the 110 and 170 °C nanoplatelets with out-of-plane thickness statistics provided in the Supporting Information. The lateral size uncertainties represent the standard deviations of the extracted size distributions (see Supporting Information). No strong dependence of lateral size on nanoplatelet thickness was observed (see Supporting Information).

https://doi.org/10.1021/acsnano.0c09244
ACS Nano 2021, 15, 6499−6506

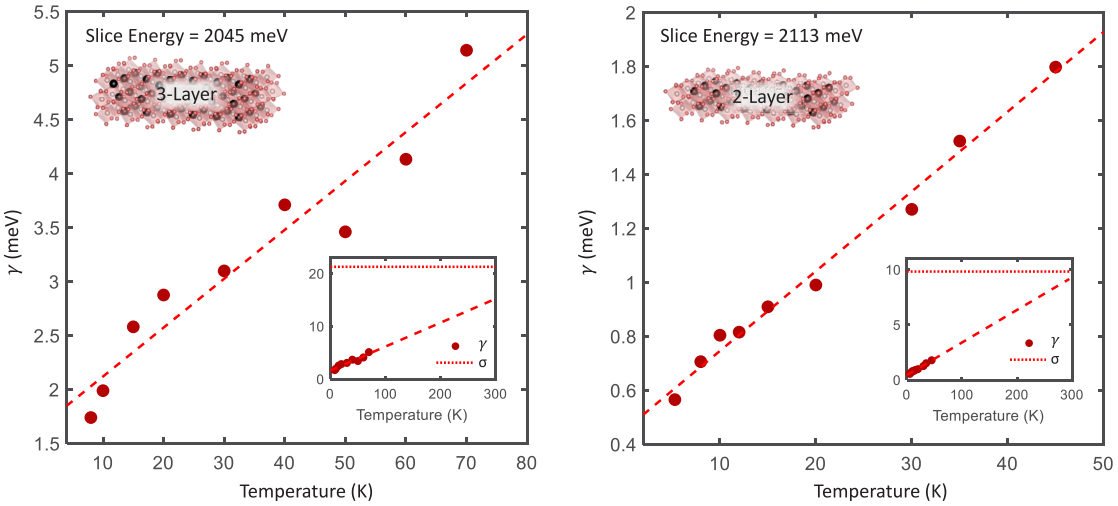

Figure 4. Dependence of the fitted homogeneous line widths on temperature for three-layer (left) and two-layer (right) nanoplatelets synthesized at a reaction temperature of 170 °C. Experimental parameters are the same as in Figure 3. The homogeneous line widths for both samples follow linear temperature dependences. The linear fits shown are $\gamma = 1.67 + (0.045)T$ meV (three-layer) and $\gamma = 0.45 + (0.032)T$ meV (two-layer). The values of γ and σ extrapolated to room-temperature are plotted in the inset. The inhomogeneous line widths, found by fitting the low-temperature absorption peaks to Voigt lineshapes as described in the text, are $\sigma = 21.32$ meV (three-layer) and $\sigma = 9.84$ meV (two-layer) and plotted as horizontal dotted lines in the insets. We note that the maximum two-layer measurement temperature of 45 K is limited by a combination of the increase in resonance energy with temperature[34] and the tuning range of our excitation laser.

Thermal Dephasing. Magnitude 2D spectra of three-layer and two-layer nanoplatelets are shown in Figure 3a,c, respectively. The vertical and horizontal axes represent the absorption and emission energies of the colloidal nanoplatelets as indicated, and the negative absorption energies reflect inverse phase evolution between delays τ and t. The diagonally elongated lineshapes indicate that despite dominant out-of-plane quantum confinement exciton resonances in perovskite nanoplatelets still possess inhomogeneous broadening due to varying confinement of lateral exciton center-of-mass motion. The degree of inhomogeneous broadening depends strongly on layer thickness, which is evident from the difference in diagonal widths between Figure 3a,c.

With increasing temperature, the lineshapes in the cross-diagonal direction broaden, which is characteristic of thermal dephasing due to elastic exciton−phonon scattering.[30,31] Specifically, first-order exciton−phonon scattering processes result in broadening that may be modeled by a linear temperature dependence for the homogeneous line width[32]

$$\gamma(T, N_X) = \gamma_0(N_X) + AT \quad (1)$$

where $\gamma_0(N_X)$ is the zero-temperature line width at a given excitation density N_X and the second term represents coupling to low-energy acoustic phonon modes with coupling strength A. In anticipation of the experimental line width temperature dependence, we neglect broadening due to discrete optical phonon modes that result in a nonlinear increase.[33] To quantify thermal broadening in each system, we plot cross-diagonal slices centered at $\hbar\omega_{CD}$ = 2045 and 2113 meV in Figure 3b,d, which reflect homogeneous broadening of nanoplatelets with resonance energy $\hbar\omega_{CD}$. The lineshapes fit well to expressions derived for exponential dephasing in the Markovian limit.[21] As the nanoplatelet bandgaps blue-shift with increasing temperature, we adjust the slice locations by a commensurate energy.

The temperature-dependent values of the homogeneous line width γ (each fitted from a 2D spectrum taken at its respective temperature) are plotted in Figure 4. By extrapolating to zero-temperature, we find different intrinsic line widths of γ_0 = 0.45 meV (170 °C two-layer) and 2.10/1.67 meV (110/170 °C three-layer). These values are comparable to measured homogeneous line widths of single CdSe nanoplatelets (γ = 0.2 meV at 20 K[35]) and single $CsPbBr_3$ nanoplatelets (γ = 0.47 meV at 5 K[27]). To explain the surprising difference in line widths between the different thicknesses, we note that optical line widths are fundamentally limited by the excited population relaxation rate. In CdSe colloidal nanospheres and nanoplatelets, the dominant population relaxation channel is a spin-flip process between an optically active bright-exciton manifold and an optically inactive dark state which inhibits light-emission.[28,36,37] Waiting time dependence of the integrated FWM signal reveals biexponential population relaxation dynamics, which indicates that this model also applies to perovskite nanoplatelets (see Supporting Information). Decreasing nanoplatelet thickness (increasing electron−hole exchange interaction) results in a larger bright-dark energy splitting,[28] and consequently a slower spin-flip relaxation rate. The line width also increases linearly with temperature, which is characteristic of acoustic phonon coupling as described by eq 1. The thermal dephasing parameters extracted from the linear fits shown in Figure 4 are A = 0.032 meV/K (two-layer) and A = 0.045 meV/K (three-layer), which indicate relatively weaker acoustic phonon coupling in the former. Weaker vibrational coupling in two-layer nanoplatelets is also reflected in their smaller thermal band gap renormalization shown in Figure 2 in which the exciton absorption peak center energy shifts by 31 meV for the three-layer nanoplatelets and only 16 meV for the two-layer nanoplatelets. Both values are comparable to that of similar two-dimensional systems such as monolayer WSe_2 (0.06 meV/K)[30] and quantum wells (~0.01 meV/K).[38]

Although optical phonon coupling is not manifest in the temperature regime shown in Figures 3 and 4, it is worth considering their possible effects at higher temperatures. There are two main pieces of evidence that point toward negligible optical phonon coupling in $CsPbI_3$ nanoplatelets, even at

https://doi.org/10.1021/acsnano.0c09244
ACS Nano 2021, 15, 6499−6506

higher temperatures. First, in recent works on MDCS of $CsPbI_3$ nanocubes,[19] clear sidebands (the equivalent of phonon replicas) were observed due to electron−phonon coupling involving optical phonons.[39] This is qualitatively different from the multidimensional spectra of $CsPbI_3$ nanoplatelets studied here, which always exhibit a single, inhomogeneously broadened peak. Second, another signature of electronic coupling to optical phonons is in the thermal band gap renormalization. This was the subject of previous work[34] which examined the shifts in absorption resonances of $CsPbI_3$ nanocubes and nanoplatelets. While the nanocubes exhibited highly nonlinear shifts in absorption energy with temperature (see also ref 40), the nanoplatelets only exhibited a linear increase in absorption energy with temperature due to acoustic phonon coupling (see Supporting Information). This behavior persists from liquid helium to room temperature, which implies a linear increase of γ up to room temperature as well. In the insets of Figure 4, we plot the inhomogeneous line width (found by fitting the absorption peaks at 10 K to Voigt profiles[41] by using our respective measured values of γ) and extrapolate the homogeneous line widths to room temperature. Although the extrapolation is not optimal due to lack of data in the intermediate temperatures, these curves lead to a rough prediction of the crossover temperature at which homogeneous broadening exceeds inhomogeneous broadening. The crossover temperatures for two-layer and three-layer nanoplatelets are 292 and 434 K, which indicate that thinner nanoplatelets are indeed homogeneously broadened at room temperature. In three-layer nanoplatelets, the extrapolated homogeneous line width at room temperature (γ(294 K) = 14.98 meV) is still significantly smaller than the inhomogeneous line width (σ = 21.32 meV), suggesting that further work is required to minimize size inhomogeneity in thick nanoplatelets for homogeneous exciton resonances at long-wavelengths.

The large inhomogeneous broadening in three-layer nanoplatelets also invites further resolving their temperature dependence analysis in terms of resonance energy, which corresponds to the cross-diagonal slice position in a 2D spectrum. The extrapolated zero-temperature homogeneous line width γ_0 is plotted in Figure 5 as a function of slice position, which exhibits an increase with increasing slice position (resonance energy). The slice position (resonance energy) dependence of the thermal dephasing parameter A is then plotted for both samples in Figure 5 which appear to vary inversely with γ_0. These trends undoubtedly relate to edge effects, since the resonance energy distribution may be directly related to the size and shape anisotropy in the lateral direction. Furthermore, the average edge length of the 110 °C nanoplatelets is 10.7 nm which approaches the exciton Bohr diameter in $CsPbI_3$ (which is half of its bulk value of 12 nm[25] for an ideal two-dimensional system). The inflection point near 2047 meV may therefore arise from a change in lateral confinement regime. In the weak confinement regime of the 170 °C sample, the intrinsic line width decreases while the thermal broadening parameter increases with shrinking nanoplatelet area. The inverse is true for the intermediate confinement regime of the 110 °C sample, which indicates different underlying physics that determine the exciton dephasing dynamics.

Excitation-Induced Dephasing. Another dominant extrinsic dephasing mechanism in semiconductors is excitation-induced dephasing (EID),[30,42,43] which arises from electronic

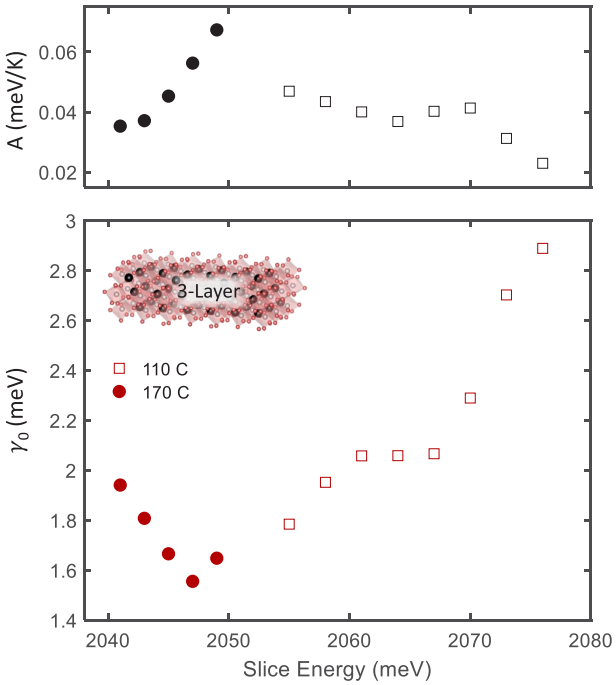

Figure 5. Dependence of the zero-temperature line width γ_0 (bottom plot) and thermal broadening parameter A (top plot) on slice position for both three-layer samples synthesized at 110 and 170 °C reaction temperatures. The values γ_0 are found by extrapolating the fitted line widths to zero-temperature, as shown in Figure 4.

many-body interactions. MDCS is ideal for studying EID, as exciton and biexciton dynamics are well-separated in both the temporal and spectral domains (see Supporting Information). Our narrow excitation bandwidths, well-matched to the probed exciton resonances, restricts the source of EID to exciton−exciton scattering.[30,44] In two-dimensional systems, this may be described by a linear dependence on excitation density N_X for the homogeneous line width

$$\gamma(T, N_X) = \gamma(T) + BN_X \quad (2)$$

where $\gamma(T)$ is the zero-density line width at temperature T and B is the exciton−exciton interaction strength. The excitation densities are calculated from the experimental laser parameters and sample optical density.

The homogeneous line width at 10 K is plotted in Figure 6a as a function of excitation density for both two-layer and three-layer nanoplatelets. We find that the line width increases linearly with excitation density for both thicknesses and reaction temperatures, a clear signature of EID, as described by eq 2. The EID parameter B for three-layer nanoplatelets synthesized at both temperatures is then plotted as a function of slice location in Figure 6b, which, most notably, exhibits a rapid increase in EID below 2055 meV. The sharp increase in EID with decreasing resonance energy for 170 °C nanoplatelets may be understood by noting the linear dependence of absorption cross-section on lateral area[45] and by considering the effect of nanoplatelet size on multiple exciton dynamics. In large nanoplatelets (smaller resonance energy) multiple excitons may form, which may then undergo scattering events that result in EID. This explains the increase in EID with decreasing slice energy below 2055 meV. The observed increase in EID beyond 2055 meV (with decreasing nano-

https://doi.org/10.1021/acsnano.0c09244
ACS Nano 2021, 15, 6499−6506

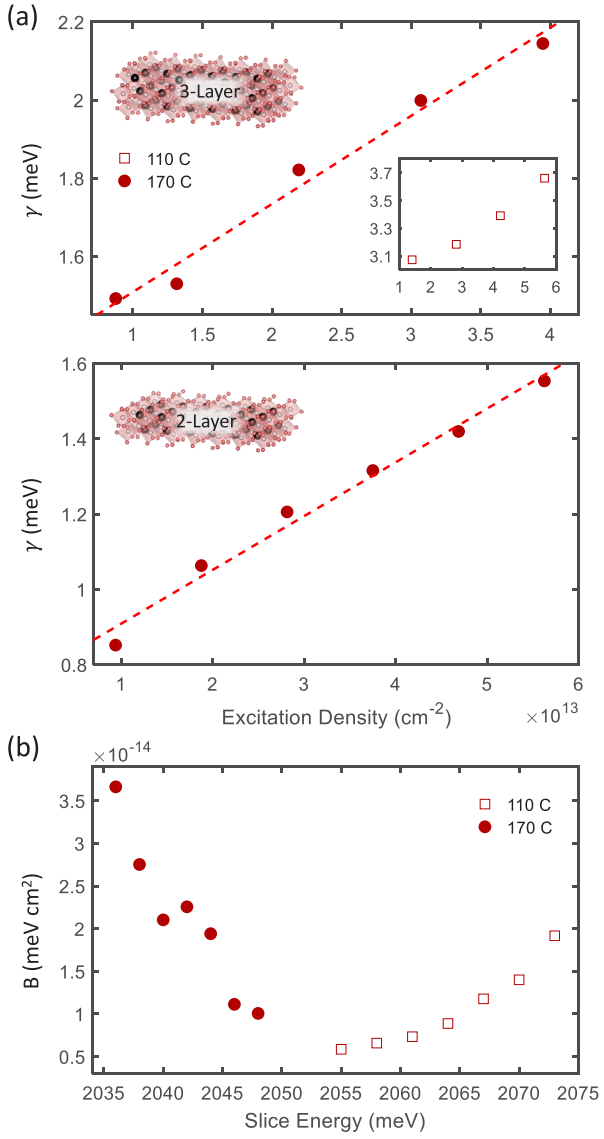

Figure 6. (a) Fitted values of the homogeneous line width as a function of excitation density for three-layer (top) and two-layer (bottom) nanoplatelets at 10 K. The three-layer line widths are fitted from slices taken at 2070 meV (110 °C, inset) and 2042 meV (170 °C) whereas the two-layer line widths are fitted from slices at 2113 meV. (b) Dependence of the EID parameter *B* on slice position in three-layer nanoplatelets.

platelet size) is unexpected, which we speculate as due to polaronic effects that result in increasing sensitivity to EID.[46] Because the nanoplatelet size is still comparable to the exciton Bohr diameter, the EID parameters measured here are much smaller than the EID parameter in, for example, monolayer WSe_2 (2.7×10^{-12} meV cm^2[30]). We note that the EID parameters measured for two-layer nanoplatelets (see Supporting Information), for example $B = 1.43 \times 10^{-14}$ meV cm^2 at $|\hbar\omega_\tau| = |\hbar\omega_t| = 2113$ meV, lie between the range of values measured for three-layer nanoplatelets synthesized at the same temperature, which indicates minimal effect of nanoplatelet thickness on EID in this size regime.

CONCLUSIONS

In conclusion, we have measured the intrinsic homogeneous line width and its broadening mechanisms in $CsPbI_3$ perovskite nanoplatelets as a function of platelet geometry. By informing the relevant design parameters for optical resonances, our results are directly relevant for implementing colloidal nanoplatelets in practical devices. For example, we find that large-area nanoplatelets offer advantages such as narrow intrinsic homogeneous line widths and lower thermal broadening and are therefore likely to be advantageous in coherent optoelectronic devices. However, small-area nanoplatelets (that suppress multiple exciton formation) may be required for narrow and stable exciton resonances in high optical intensity applications. We realize the narrowest, sub-milli-electronvolts intrinsic line widths by reducing the nanoplatelet thickness to a mere three polyhedral layers, which represents an important step toward engineering ideal atomlike emission from colloidal materials.

METHODS

$CsPbI_3$ Nanoplatelet Synthesis Method. $CsPbI_3$ nanoplatelets were synthesized according to a procedure detailed elsewhere.[26] Briefly, 15 mg of Cs_2CO_3 and 158 mg of $Pb(acetate)_2 3H_2O$ were loaded into 50 mL, 3-neck flask along with 1 mL of oleic acid (OA), 0.5 mL of oleylamine (OLA) and 4.5 mL of 1-octadecene (1-ODE). The mixture was kept at 100 °C for 1 h under reduced pressure. After complete degassing of the mixture, the system was kept under nitrogen flowing and heated-up until the specified reaction temperature (either 110 or 170 °C). Then, a solution containing 130 mg of SnI_4 in 1 mL of 1-ODE, 0.5 mL of OA, and 0.5 mL of OLA (all solvents were predegassed before using) was swiftly injected. The mixture was rapidly placed into a water bath until room temperature. The nanoplatelets were separated from the crude solution by centrifugation at 13 500 rpm for 10 min and resuspended with anhydrous *n*-hexane.

Cryogenic Temperature Measurements. The $CsPbI_3$ nanoplatelets are suspended in heptamethylnonane, a branched alkane that forms a transparent glass at temperatures below 100 K. Importantly, perovskite nanocrystals may degrade due to interactions with their environment. To minimize such effects, the samples, held in a sealed beaker, were stored in a dark refrigerator for the duration of their lifetime. Upon each experimental measurement, a subset of the nanoplatelets was pipetted out of the main beaker and loaded between two sapphire windows in a custom sample holder approximately 0.5 mm thick, which is then mounted to a liquid helium coldfinger cryostat and cooled to cryogenic temperatures.

MDCS Measurements. The excitation laser pulses used to perform multidimensional coherent spectroscopy (MDCS) are generated at a 250 kHz repetition rate by an optical parameteric amplifier (Coherent OPA 9400) pumped by a regenerative Ti:sapphire amplifier (Coherent RegA 9000). The FWM signal is isolated by wave-vector phase-matching in the box geometry (shown in Figure 1b), measured via spectral interferometry[47] with a fourth phase-stabilized local oscillator pulse. All pulses are colinearly polarized and measured to be approximately 70 fs in duration via intensity autocorrelation.

Exciton Density Calculation. To calculate the exciton excitation density, we use

$$N_X = \frac{P_{avg}(1 - 10^{-OD})}{\pi r^2 f_{rep} E_{ph}} \quad (3)$$

where P_{avg} is the average power per excitation beam, $A = 1-10^{-OD}$ is the linear absorbance of each respective nanoplatelet ensemble, $r = 55$ μm is the focused beam radius at the sample, $f_{rep} = 250$ kHz is the excitation repetition rate, and E_{ph} is the excitation photon energy.

https://doi.org/10.1021/acsnano.0c09244
ACS Nano 2021, 15, 6499−6506

ASSOCIATED CONTENT

Supporting Information

The Supporting Information is available free of charge at https://pubs.acs.org/doi/10.1021/acsnano.0c09244.

TEM and spectroscopic characterization of nanoplatelet thickness; TEM characterization of nanoplatelet lateral size; waiting time dependence of integrated four-wave-mixing signal; waiting time dependence of homogeneous line width; linear and four-wave-mixing data of 110 °C sample; resonance energy temperature dependence of two- and three-layer nanoplatelets; resonance energy dependence of EID in two-layer nanoplatelets; additional discussion concerning effect of varying exciton/biexciton quantum yield (PDF)

AUTHOR INFORMATION

Corresponding Authors

Lazaro A. Padilha − *Instituto de Fisica Gleb Wataghin, Universidade Estadual de Campinas, Campinas, Sao Paulo 13083-970, Brazil;* orcid.org/0000-0002-8825-6611; Email: padilha@ifi.unicamp.br

Steven T. Cundiff − *Department of Physics, University of Michigan, Ann Arbor, Michigan 48109, United States;* orcid.org/0000-0002-7119-5197; Email: cundiff@umich.edu

Authors

Albert Liu − *Department of Physics, University of Michigan, Ann Arbor, Michigan 48109, United States;* orcid.org/0000-0001-6718-3719

Gabriel Nagamine − *Instituto de Fisica Gleb Wataghin, Universidade Estadual de Campinas, Campinas, Sao Paulo 13083-970, Brazil;* orcid.org/0000-0002-4830-7357

Luiz G. Bonato − *Instituto de Quimica, Universidade Estadual de Campinas, Campinas, Sao Paulo 13083-970, Brazil*

Diogo B. Almeida − *Instituto de Fisica Gleb Wataghin, Universidade Estadual de Campinas, Campinas, Sao Paulo 13083-970, Brazil*

Luiz F. Zagonel − *Instituto de Fisica Gleb Wataghin, Universidade Estadual de Campinas, Campinas, Sao Paulo 13083-970, Brazil;* orcid.org/0000-0002-4043-0318

Ana F. Nogueira − *Instituto de Quimica, Universidade Estadual de Campinas, Campinas, Sao Paulo 13083-970, Brazil;* orcid.org/0000-0002-0838-7962

Complete contact information is available at: https://pubs.acs.org/10.1021/acsnano.0c09244

Notes

The authors declare no competing financial interest.

ACKNOWLEDGMENTS

We acknowledge M. Siemens for fruitful discussions. This work was supported by the Department of Energy Grant DE-SC0015782. G.N. and D.B.A. acknowledge support by fellowships from the Brazilian National Council for Scientific and Technological Development (CNPq). D.B.A. acknowledges support from FAPESP (project number 2019/22576-8). L.A.P. acknowledges support from FAPESP (project number 2018/15574-6). Research was supported by LNNano/CNPEM/MCTIC, where the TEM measurements were performed.

REFERENCES

(1) Herz, L. M. Charge-Carrier Dynamics in Organic-Inorganic Metal Halide Perovskites. *Annu. Rev. Phys. Chem.* **2016**, *67*, 65−89.

(2) Lozano, G. The Role of Metal Halide Perovskites in Next-Generation Lighting Devices. *J. Phys. Chem. Lett.* **2018**, *9*, 3987−3997.

(3) Zhao, Z.; Gu, F.; Rao, H.; Ye, S.; Liu, Z.; Bian, Z.; Huang, C. Metal Halide Perovskite Materials for Solar Cells with Long-Term Stability. *Adv. Energy Mater.* **2019**, *9*, 1802671.

(4) Fu, Y.; Zhu, H.; Chen, J.; Hautzinger, M. P.; Zhu, X.-Y.; Jin, S. Metal Halide Perovskite Nanostructures for Optoelectronic Applications and the Study of Physical Properties. *Nat. Rev. Mater.* **2019**, *4*, 169−188.

(5) Akkerman, Q. A.; Rainò, G.; Kovalenko, M. V.; Manna, L. Genesis, Challenges and Opportunities for Colloidal Lead Halide Perovskite Nanocrystals. *Nat. Mater.* **2018**, *17*, 394−405.

(6) Shamsi, J.; Urban, A. S.; Imran, M.; De Trizio, L.; Manna, L. Metal Halide Perovskite Nanocrystals: Synthesis, Post-Synthesis Modifications, and Their Optical Properties. *Chem. Rev.* **2019**, *119*, 3296−3348.

(7) Bekenstein, Y.; Koscher, B. A.; Eaton, S. W.; Yang, P.; Alivisatos, A. P. Highly Luminescent Colloidal Nanoplates of Perovskite Cesium Lead Halide and Their Oriented Assemblies. *J. Am. Chem. Soc.* **2015**, *137*, 16008−16011.

(8) Tong, Y.; Bladt, E.; Aygüler, M. F.; Manzi, A.; Milowska, K. Z.; Hintermayr, V. A.; Docampo, P.; Bals, S.; Urban, A. S.; Polavarapu, L.; Feldmann, J. Highly Luminescent Cesium Lead Halide Perovskite Nanocrystals with Tunable Composition and Thickness by Ultrasonication. *Angew. Chem., Int. Ed.* **2016**, *55*, 13887−13892.

(9) Jurow, M. J.; Morgenstern, T.; Eisler, C.; Kang, J.; Penzo, E.; Do, M.; Engelmayer, M.; Osowiecki, W. T.; Bekenstein, Y.; Tassone, C.; Wang, L.-W.; Alivisatos, A. P.; Brütting, W.; Liu, Y. Manipulating the Transition Dipole Moment of CsPbBr3 Perovskite Nanocrystals for Superior Optical Properties. *Nano Lett.* **2019**, *19*, 2489−2496.

(10) Rowland, C. E.; Fedin, I.; Zhang, H.; Gray, S. K.; Govorov, A. O.; Talapin, D. V.; Schaller, R. D. Picosecond Energy Transfer and Multiexciton Transfer Outpaces Auger Recombination in Binary CdSe Nanoplatelet Solids. *Nat. Mater.* **2015**, *14*, 484.

(11) Weidman, M. C.; Seitz, M.; Stranks, S. D.; Tisdale, W. A. Highly Tunable Colloidal Perovskite Nanoplatelets through Variable Cation, Metal, and Halide Composition. *ACS Nano* **2016**, *10*, 7830−7839.

(12) Li, M.; Zhi, M.; Zhu, H.; Wu, W.-Y.; Xu, Q.-H.; Jhon, M. H.; Chan, Y. Ultralow-Threshold Multiphoton-Pumped Lasing from Colloidal Nanoplatelets in Solution. *Nat. Commun.* **2015**, *6*, 8513.

(13) Cundiff, S. T.; Mukamel, S. Optical Multidimensional Coherent Spectroscopy. *Phys. Today* **2013**, *66*, 44−49.

(14) Gellen, T. A.; Lem, J.; Turner, D. B. Probing Homogeneous Line Broadening in CdSe Nanocrystals Using Multidimensional Electronic Spectroscopy. *Nano Lett.* **2017**, *17*, 2809−2815.

(15) Seiler, H.; Palato, S.; Sonnichsen, C.; Baker, H.; Kambhampati, P. Seeing Multiexcitons through Sample Inhomogeneity: Band-Edge Biexciton Structure in CdSe Nanocrystals Revealed by Two-Dimensional Electronic Spectroscopy. *Nano Lett.* **2018**, *18*, 2999−3006.

(16) Liu, A.; Almeida, D. B.; Bae, W. K.; Padilha, L. A.; Cundiff, S. T. Non-Markovian Exciton-Phonon Interactions in Core-Shell Colloidal Quantum Dots at Femtosecond Timescales. *Phys. Rev. Lett.* **2019**, *123*, 057403.

(17) Liu, A.; Almeida, D. B.; Bae, W.-K.; Padilha, L. A.; Cundiff, S. T. Simultaneous Existence of Confined and Delocalized Vibrational Modes in Colloidal Quantum Dots. *J. Phys. Chem. Lett.* **2019**, *10*, 6144−6150.

(18) Seiler, H.; Palato, S.; Sonnichsen, C.; Baker, H.; Socie, E.; Strandell, D. P.; Kambhampati, P. Two-Dimensional Electronic Spectroscopy Reveals Liquid-Like Lineshape Dynamics in CsPbI3 Perovskite Nanocrystals. *Nat. Commun.* **2019**, *10*, 4962.

(19) Liu, A.; Almeida, D. B.; Bonato, L. G.; Nagamine, G.; Zagonel, L. F.; Nogueira, A. F.; Padilha, L. A.; Cundiff, S. T. Multidimensional

Coherent Spectroscopy Reveals Triplet State Coherences in Cesium Lead-Halide Perovskite Nanocrystals. *Sci. Adv.* **2021**, *7*, eabb3594.
(20) Bristow, A. D.; Karaiskaj, D.; Dai, X.; Zhang, T.; Carlsson, C.; Hagen, K. R.; Jimenez, R.; Cundiff, S. T. A Versatile Ultrastable Platform for Optical Multidimensional Fourier-Transform Spectroscopy. *Rev. Sci. Instrum.* **2009**, *80*, 073108.
(21) Siemens, M. E.; Moody, G.; Li, H.; Bristow, A. D.; Cundiff, S. T. Resonance Lineshapes in Two-Dimensional Fourier Transform Spectroscopy. *Opt. Express* **2010**, *18*, 17699−17708.
(22) Bohn, B. J.; Simon, T.; Gramlich, M.; Richter, A. F.; Polavarapu, L.; Urban, A. S.; Feldmann, J. Dephasing and Quantum Beating of Excitons in Methylammonium Lead Iodide Perovskite Nanoplatelets. *ACS Photonics* **2018**, *5*, 648−654.
(23) Smallwood, C. L.; Autry, T. M.; Cundiff, S. T. Analytical Solutions to the Finite-Pulse Bloch Model for Multidimensional Coherent Spectroscopy. *J. Opt. Soc. Am. B* **2017**, *34*, 419−429.
(24) Do, T. N.; Gelin, M. F.; Tan, H.-S. Simplified Expressions that Incorporate Finite Pulse Effects into Coherent Two-Dimensional Optical Spectra. *J. Chem. Phys.* **2017**, *147*, 144103.
(25) Protesescu, L.; Yakunin, S.; Bodnarchuk, M. I.; Krieg, F.; Caputo, R.; Hendon, C. H.; Yang, R. X.; Walsh, A.; Kovalenko, M. V. Nanocrystals of Cesium Lead Halide Perovskites (CsPbX3, X = Cl, Br, and I): Novel Optoelectronic Materials Showing Bright Emission with Wide Color Gamut. *Nano Lett.* **2015**, *15*, 3692−3696.
(26) Bonato, L. G.; Moral, R. F.; Nagamine, G.; Alo, A.; Germino, J. C.; da Silva, D. S.; Almeida, D. B.; Zagonel, L. F.; Galembeck, F.; Padilha, L. A.; Nogueira, A. F. Revealing the Role of Tin(IV) Halides in the Anisotropic Growth of CsPbX3 Perovskite Nanoplates. *Angew. Chem., Int. Ed.* **2020**, *59* (28), 11501−11509.
(27) Huo, C.; Fong, C. F.; Amara, M.-R.; Huang, Y.; Chen, B.; Zhang, H.; Guo, L.; Li, H.; Huang, W.; Diederichs, C.; Xiong, Q. Optical Spectroscopy of Single Colloidal CsPbBr3 Perovskite Nanoplatelets. *Nano Lett.* **2020**, *20*, 3673−3680.
(28) Shornikova, E. V.; Biadala, L.; Yakovlev, D. R.; Sapega, V. F.; Kusrayev, Y. G.; Mitioglu, A. A.; Ballottin, M. V.; Christianen, P. C. M.; Belykh, V. V.; Kochiev, M. V.; Sibeldin, N. N.; Golovatenko, A. A.; Rodina, A. V.; Gippius, N. A.; Kuntzmann, A.; Jiang, Y.; Nasilowski, M.; Dubertret, B.; Bayer, M. Addressing the Exciton Fine Structure in Colloidal Nanocrystals: The Case of CdSe Nanoplatelets. *Nanoscale* **2018**, *10*, 646−656.
(29) Becker, M. A.; Vaxenburg, R.; Nedelcu, G.; Sercel, P. C.; Shabaev, A.; Mehl, M. J.; Michopoulos, J. G.; Lambrakos, S. G.; Bernstein, N.; Lyons, J. L.; Stöferle, T.; Mahrt, R. F.; Kovalenko, M. V.; Norris, D. J.; Rain_o, G.; Efros, A. L. Bright Triplet Excitons in Caesium Lead Halide Perovskites. *Nature* **2018**, *553*, 189−193.
(30) Moody, G.; Kavir Dass, C.; Hao, K.; Chen, C.-H.; Li, L.-J.; Singh, A.; Tran, K.; Clark, G.; Xu, X.; Berghauser, G.; Malic, E.; Knorr, A.; Li, X. Intrinsic Homogeneous Linewidth and Broadening Mechanisms of Excitons in Monolayer Transition Metal Dichalcogenides. *Nat. Commun.* **2015**, *6*, 8315.
(31) Singh, R.; Autry, T. M.; Nardin, G.; Moody, G.; Li, H.; Pierz, K.; Bieler, M.; Cundiff, S. T. Anisotropic Homogeneous Linewidth of the Heavy-Hole Exciton in (110)-Oriented GaAs Quantum Wells. *Phys. Rev. B: Condens. Matter Mater. Phys.* **2013**, *88*, 045304.
(32) Rudin, S.; Reinecke, T. L.; Segall, B. Temperature-Dependent Exciton Linewidths in Semiconductors. *Phys. Rev. B: Condens. Matter Mater. Phys.* **1990**, *42*, 11218−11231.
(33) Liu, A.; Cundiff, S. T.; Almeida, D. B.; Ulbricht, R. Spectral Broadening and Ultrafast Dynamics of a Nitrogen-Vacancy Center Ensemble in Diamond. Accepted for publication in *Materials for Quantum Technology*;**2021**.
(34) Liu, A.; Bonato, L. G.; Sessa, F.; Almeida, D. B.; Isele, E.; Nagamine, G.; Zagonel, L. F.; Nogueira, A. F.; Padilha, L. A.; Cundiff, S. T. Effect of Dimensionality on the Optical Absorption Properties of CsPbI3 Perovskite Nanocrystals. *J. Chem. Phys.* **2019**, *151*, 191103.
(35) Tessier, M. D.; Javaux, C.; Maksimovic, I.; Loriette, V.; Dubertret, B. Spectroscopy of Single CdSe Nanoplatelets. *ACS Nano* **2012**, *6*, 6751−6758.
(36) Accanto, N.; Masia, F.; Moreels, I.; Hens, Z.; Langbein, W.; Borri, P. Engineering the Spin−Flip Limited Exciton Dephasing in Colloidal CdSe/CdS Quantum Dots. *ACS Nano* **2012**, *6*, 5227−5233.
(37) Masia, F.; Accanto, N.; Langbein, W.; Borri, P. Spin-Flip Limited Exciton Dephasing in CdSe/ZnS Colloidal Quantum Dots. *Phys. Rev. Lett.* **2012**, *108*, 087401.
(38) Schultheis, L.; Honold, A.; Kuhl, J.; Köhler, K.; Tu, C. W. Optical Dephasing of Homogeneously Broadened Two-Dimensional Exciton Transitions in GaAs Quantum Wells. *Phys. Rev. B: Condens. Matter Mater. Phys.* **1986**, *34*, 9027−9030.
(39) Liu, A.; Cundiff, S. T. Spectroscopic Signatures of Electron-Phonon Coupling in Silicon-Vacancy Centers in Diamond. *Phys. Rev. Mater.* **2020**, *4*, 055202.
(40) Saran, R.; Heuer-Jungemann, A.; Kanaras, A. G.; Curry, R. J. Giant Bandgap Renormalization and Exciton−Phonon Scattering in Perovskite Nanocrystals. *Adv. Opt. Mater.* **2017**, *5*, 1700231.
(41) Whiting, E. E. An Empirical Approximation to the Voigt Profile. *J. Quant. Spectrosc. Radiat. Transfer* **1968**, *8*, 1379−1384.
(42) Wang, H.; Ferrio, K. B.; Steel, D. G.; Berman, P. R.; Hu, Y. Z.; Binder, R.; Koch, S. W. Transient Four-Wave-Mixing Line Shapes: Effects of Excitation-Induced Dephasing. *Phys. Rev. A: At., Mol., Opt. Phys.* **1994**, *49*, R1551−R1554.
(43) Shacklette, J. M.; Cundiff, S. T. Role of Excitation-Induced Shift in the Coherent Optical Response of Semiconductors. *Phys. Rev. B: Condens. Matter Mater. Phys.* **2002**, *66*, 045309.
(44) Schultheis, L.; Kuhl, J.; Honold, A.; Tu, C. W. Ultrafast Phase Relaxation of Excitons via Exciton-Exciton and Exciton-Electron Collisions. *Phys. Rev. Lett.* **1986**, *57*, 1635−1638.
(45) Yeltik, A.; Delikanli, S.; Olutas, M.; Kelestemur, Y.; Guzelturk, B.; Demir, H. V. Experimental Determination of the Absorption Cross-Section and Molar Extinction Coefficient of Colloidal CdSe Nanoplatelets. *J. Phys. Chem. C* **2015**, *119*, 26768−26775.
(46) Roy, C.; Hughes, S. Influence of Electron−Acoustic-Phonon Scattering on Intensity Power Broadening in a Coherently Driven Quantum-Dot−Cavity System. *Phys. Rev. X* **2011**, *1*, 021009.
(47) Lepetit, L.; Chériaux, G.; Joffre, M. Linear Techniques of Phase Measurement by Femtosecond Spectral Interferometry for Applications in Spectroscopy. *J. Opt. Soc. Am. B* **1995**, *12*, 2467−2474.

https://doi.org/10.1021/acsnano.0c09244
ACS Nano 2021, 15, 6499−6506